J Nanostruct 13(1): 223-237, Winter 2023

RESEARCH PAPER

Hydrogel Nanocomposite of Acrylic Acid-Grafted Sodium Alginate-Based Zinc Oxide: Synthesis, Characterization, and Applicability for Crystal Violet Dye Removal

*Aseel M. Aljeboree [1], Hadeel K. Albdairi [2], Usama S. Altimari [3], Noor Abd Alkhudhur Salman [4], Abbas Washeel Salman [5], Ayad F. Alkaim [1]**

[1] *Department of Chemistry, College of Sciences for women, University of Babylon, Hilla, Iraq*

[2] *Ministry of Interior Affairs ,Babylon Police command, Criminal evidence investigation department, Babylon Province, Hilla, Iraq*

[3] *Department of Medical Laboratories Technology, Al-Nisour University College, Baghdad, Iraq*

[4] *College of Pharmacy, National University of Science and Technology, Dhi Qar, Iraq*

[5] *Department of Production, College of Agriculture, Wasit University, Kut, Wasit, Iraq*

ARTICLE INFO

Article History:
Received 19 September 2022
Accepted 18 December 2022
Published 01 January 2023

Keywords:
Adsorption
Crystal Violet
Hydrogel Polymer
Sodium alginate
Zinc oxide

ABSTRACT

In this current research work, hydrogel composite polymer of sodium alginate-g-(polyacrylicacid-co-Sodium4-vinylbenzenesulfonate)/zinic oxide hydrogel (SA-g-(PAAc-co-VBS)/ZnO has been synthesized to be an efficient adsorbent for cationic dye namely crystal violet (CV). The physicochemical properties of the synthesized compound were identified via several characterization techniques such as Fourier transform infrared (FTIR), Field emission scanning electron microscope (FE-SEM), Thermo gravimetric analysis (TGA), X-ray diffraction (XRD), and Transmission electron microscopes (TEM). The adsorption kinetics and equilibrium isotherm of (SA-g-(PAAC-co-VBS)/ZnO towards CV removal were best fitted the pseudo-first-order and Freundlich isotherm models respectively (Qe =956.56 mg/g) at optimum condition temperatures 30 °C, Conc.= 200 mg. L^{-1}, pH= 6.6, and weight of surface 0.04 g/100 ml. Recyclability and Desorption studies indicated the best recycling performance at 3 cycles of using (SA-g-(PAAC-co-VBS)/ZnO), with a significant efficiency >80%. Depend on the results, the synthesized SA-g-(PAAc-co-VBS)/ZnO can be applied as a promising, eco-friendly, cost-effective, and efficient adsorbent for cationic dye removal.

How to cite this article
Aljeboree A M., Albdairi H K., Altimari U S. et al. Hydrogel Nanocomposite of Acrylic Acid-Grafted Sodium Alginate-Based Zinc Oxide: Synthesis, Characterization, and Applicability for Crystal Violet Dye Removal. J Nanostruct, 2023; 13(1):223-237.
DOI: 10.22052/JNS.2023.01.024

INTRODUCTION

Textile dyes industries operations utilize plenty of water and thus cast large amounts of wastewater. The harmful effects of dyes on the body in the water are not confirmed to be toxic but may cause a reduction of dissolved oxygen and obstruction of the photosynthetic processes [1]. In this regard, several treatment methods such as ozonation [2], coagulation/flocculation [3], filtration membrane [4], liquid-liquid extraction [5], photocatalysis [6], and adsorption [7] have been applied in removing dyes from aqueous media. Thus, the adsorption

* *Corresponding Author Email: alkaimayad@gmail.com*

process is of utmost preferred in water treatment due to its high efficiency, design simplicity, low cost, and non-toxicity. The adsorptive removal of the water contaminants depends on several significant factors such as the molecular structure of the contaminants, the nature and functionality of the adsorbent, and key operational conditions. The network structure is the main characteristic of super-adsorbent polymers that have a suitable degree of cross-linking. These polymers can form a very stable hydrogel by absorbing and retaining very large amounts of aqueous solutions or water. Thus retained water is hard to remove under pressure. Currently, they are utilized in several applications having hygienic products agriculture, sealing, food additives, pharmaceuticals, drug release systems, regenerative medicines, coal de-watering, artificial snow, biomedical applications tissue engineering, wound dressing separation of biomolecules or cells, diagnostics, and barrier materials to regulate biological adhesions biosensor [8-11].

Different prepared composites were used in the removal of dyes or other pollutants. Nejhad and co-workers utilized Poly(vinyl alcohol)/ Montmorillonite nanocomposite hydrogels in the removal of the Methylene Blue from aqueous solution solutions [12]. In their study, they found that the dependency of gel content and swelling of the nanocomposite hydrogel adsorbent is in direct and inverse proportion to the amount of the incorporated montmorillonite to the adsorbent, respectively. Jawad and co-workers synthesized a cross-linked chitosan-epichlorohydrin/TiO_2 bioadsorbent nanocomposite and used it to remove the reactive red 120 dye from an aqueous solution with an adsorption capacity of 210 mg/g at 30 °C [13]. They also synthesized a new composite by the modification of a cross-linked chitosan-glyoxal with kaolin clay as an inorganic filler [14]. The prepared composite was applied in the color removal and COD reduction of the dye remazol brilliant blue R with the highest adsorption capacity of 447.1 mg/g at 30 °C. Our previous work reported the synthesis and DFT studies of new hydrogel nanocomposite SA-g-p(AAc-co-MA)/ TiO_2. The synthesized nanocomposite was applied as an adsorbent to remove Brilliant green dye from aqueous media, which showed promising results under the optimized conditions [15].

Due to chemical stability, low cost, very low toxicity, photostability, Highly oxidizing, and exclusive semiconducting properties, ZnO nanoparticles are vastly utilized in several applications like photo-catalysis, dye-sensitized solar cells, pigments, drug delivery, etc. Malik and co-workers studied the effect of the high stability mechanical prepared CuS-ZnO nanocomposite on the photodegradation of Congo red and phenol pollutants [16]. Under visible light, the experimental degradation of Congo red and phenol showed that CuS could aid ZnO in this process. However, there are some problems with using ZnO nanoparticles as an adsorbent in an aqueous solution such as; recovery from the solution after the reaction completion, easy aggregation, and time consumption [17]. These problems have reduced the applications of ZnO nanoparticles in water treatment. Here, we incorporated ZnO nanoparticles in the (SA-g-(PAAC-co-VBS) hydrogel matrix and utilized the product (SA-g-(PAAC-co-VBS)/ZnO for the removal of CV dye in an aqueous solution. Further, the newly synthesized adsorbent showed a significant recycling performance with an efficiency of >80%, other than its other studied properties.

MATERIALS AND METHODS

Sodium alginate (SA), Acrylic acid (AAC), N,N-methylene-bis acrylamide(MBA) , Sodium-4-vinylbenzenesulfonate(VBS), Potassium persulfate (KPS), Hydrochloric acid (HCl), Soduim hydroxide (NaOH), Ethanol(C_2H_5OH) and Zinc Oxide (ZnO) were supplied by Sigma–Aldrich. Crystal Violet(CV) is a textile dye obtained from Al- Hila factory (Iraq) for textiles (Molecular weight 407.98 g/mol , M.F $C_{25}H_3OCl$ and λmax=590 nm). A standard solution (1000 mg L^{-1}) was prepared by dissolving of 1 gm of CV in 1000 mL of distilled water.

FT-IR technique was utilized to identify functional groups on the surface which responsible for CV dye adsorption. Adsorbent surfaces (SA-g-(PAAC-co-VBS), (SA-g-(PAAC-co-VBS)/ZnO), and the after-adsorption-dye-loaded adsorbent sample was placed in an oven at 65 ◦C for 4 h. The samples were made as pellets, and the spectra of the adsorbent were recorded before and after the adsorption process in the range 4000–400 cm−1 using an Infrared spectrophotometer (FTIR, 8000, Shimadzu-Japan).

Preparation of SA-g-(PAAC-co-VBS)/ZnO) hydrogel

The hydrogel was prepared by the free radical graft copolymerization method. Sodium alginate

(SA) 1 gm was dissolved in distilled water (20 mL). In the reaction flask, a quantity of ZnO NPs (0.1g) was suspended in 20 ml of distilled water and shaken for 5 h followed by ultra-sonic for 2 h. Then, it was added to the solution sodium alginate, followed by stirring at 25 °C for 2 h until a well-dispersed homogeneous gel formed. At that point, Sodium 4-vinylbenzenesulfonate VBS (0.5 g) followed by Acrylic acid AAC (3 ml) was added with consistent blending at 25 °C. Then, potassium

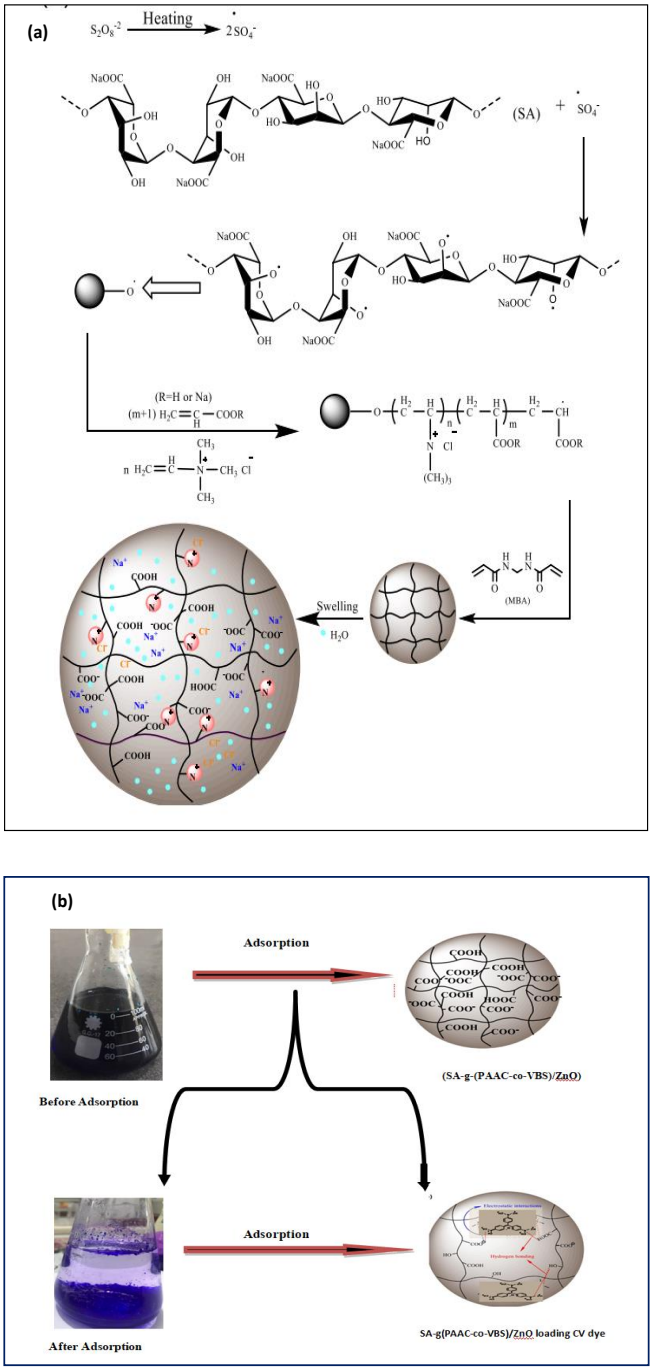

Fig. 1. Proposed mechanism of reaction and swelling of SA-g-(PAAC-co-VBS)/ ZnO (a), and schematic diagram for CV adsorption mechanism (b).

persulfate (0.03 g) in 1ml of distilled water was added with continuous mixing for 5 min. After that, N,N-methylene-bisacrylamide (MBA), (0.05 g) was added to the mixture with the a stream of N_2. Finally, the reaction flask was set in a 70 °C water bath to complete the co-polymerization and obtain the hydrogel nanocomposite (SA-g-(PAAC-co-VBS)/ZnO). The obtained hydrogel was cut into small pieces and washed with plenty of distilled water, and then with ethanol to remove unreacted chemicals, dried in an oven at 60 °C, and then kept in a desiccator.

The synthesis steps are summarized in Fig. 1a. The decomposition of the initiator generates the free radicals that are transferred to SA to initiate the polymerization of AAC and VBS. Then, the monomers are grafted onto the SA backbone. After that, the addition of the cross-linker resulted in the formation of a three-dimensional (3D) network. The proposed adsorption process of CV is shown in Fig. 1b.

Adsorption study

Batch adsorption experiments were carried out in 100 mL conical flasks, in a 100 ml solution with a 200 mg/L concentration of CV dye. To the CV solution, an amount of hydrogel 0.04 g was added. The conical flasks were shaken with a speed of 160 rpm for 2 h in a shaker water bath at room temperature. The effects of different parameters such as pH solution (3-10), contact time (2-240 min), adsorbent dosage (0.01-0.1 g), and solution temperature (25-40 °C) were studied. To analyze the residual concentration of CV dye in the solution, the samples were collected from the flask at pre-determined time intervals. Then, the residual of CV was determined using a UV-Visible spectrophotometer at λ_{max}= 590 nm. The following equation was used to obtain the amounts of adsorbed and removed CV:

$$qe = \frac{(C_0 - C_e) * V_L}{m_{gm}} \quad (1)$$

Where qe = The adsorbed dye per unit of adsorbent (mg/g).

C_0= Initial concentration ($mg.L^{-1}$), Ce= Equilibrium concentration ($mg.L^{-1}$).

m= Dose of adsorbent (g), VL= Volume of solution (L).

The removal percentage (E%) of CV was calculated based on the reduction in absorbance at λ_{max} value of the dye as follows [18]:

$$E\,\% = \frac{C_0 - C_e}{C_0} * 100 \quad (2)$$

RESULT AND DISCUSSION

FTIR spectral analysis

Infrared analysis results are shown in fig. 2. In the alginate spectrum, a broad band 3000 to 3600 cm^{-1} is attributed to the stretching of COOH groups, which showed a little change in the

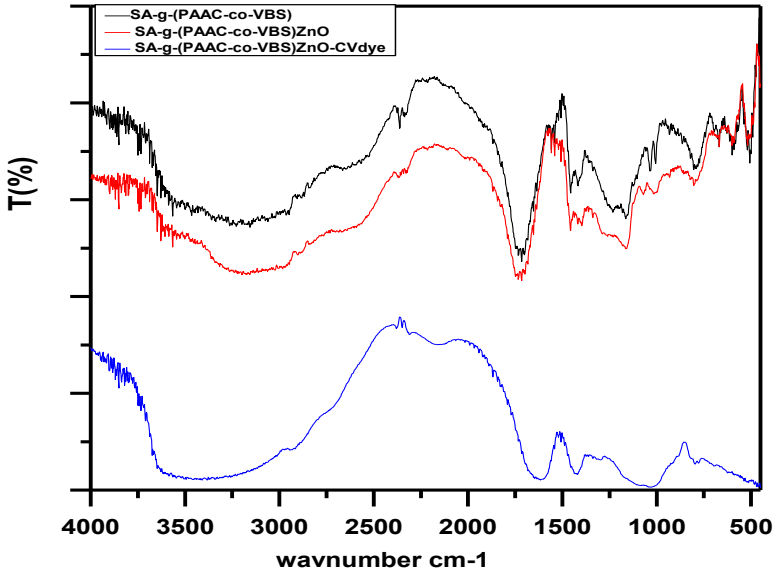

Fig. 2. FT-IR spectra of (SA-g-(PAAC-co-VBS)) and (SA-g-(PAAC-co-VBS)/ZnO) before and after adsorption of the dye .

intensity after modification with ZnO. The bands appeared at 2923-2925 cm^{-1} can be attributed to the stretching of C–H from glucose units in alginate [19]. In the spectrum of SA-g-(PAA-co-VBS)/ZnO, the characteristic band that appeared at 1718 cm^{-1} is assigned to the stretching of C=O in poly(acrylic acid), which significantly supports of grafting of AAC on SA. Moreover, the broadband at 450–800 cm^{-1} is assigned to the stretching of Zn-O-Zn groups [20, 21]. FT-IR spectra of ZnO NPs generally show two main bands, the first one at 627 cm^{-1} (corresponding to stretching of Zn–O) and the second at 1404 cm^{-1} (corresponding to stretching of Zn–O–Zn), which confirm the presence of ZnNP in SA-g-(PAA-co-VBS)/ZnO, thus the successful graft co-polymerization of SA with the ZnO NPs [22, 23].

TGA analysis

Thermogravimetric analysis of the nanocomposite was investigated at a heating up to 600 °C, with a rate of 5 ◦C/min under dry nitrogen. The result of TGA of the as-obtained Architecture-like (a) SA-g-(PAAC-co-VBS), (b) SA-g-(PAAC-co-VBS)/ZnO NPs. Architectures further provide evidence that ZnO NPs incorporated into SA-g-(PAAC-co-VBS)/ZnO NPs architectures, as shown in Fig. 3. In the TGA curve {W(mg) vs temperature T(°C) plots} [24-26], a weight loss observed in the range of 25–600 °C, in which the weight loss of 42.4%, and 52.2% in the range of 25–300 °C for SA-g-(PAAC-co-VBS) and SA-g-(PAAC-co-VBS)/ZnO NPs, respectively. This is attributed to the desorption and then evaporation of bound water. The weight loss of 25.8% in SA-g-(PAAC-co-VBS, and 49.1% in SA-g-(PAAC-co-VBS)/ZnO NPs at the range 460-580 °C and 300-580 °C indicates the loss of cross-linked network structure, and the formation of anhydride with the removal of water molecules from carboxylic groups in polymer chains. The decomposition rate of SA-g-(PAAC-co-VBS)/ZnO NPs is less than that of SA-g-(PAAC-co-VBS). TGA results predicted that ZnO could behave as a thermal barrier, therefore it increases the thermal stability of synthesized SA-g-(PAAC-co-VBS)/ZnO NPs hydrogel [27-30].

FE-SEM and TEM analysis

FE-SEM technique was used as a tool in characterizing the physical properties and surface morphology of the new adsorbent. The synthesized ZnO NPs arranged in a flower-like shape pattern as shown in Fig. 4a. The pores give a substantial chance for ZnO NPs to entangle inside them [31]. The rough porous surface of (SA-g-(PAAC-co-VBS) and (SA-g-(PAAC-co-VBS)/ZnO) revealed changes in the morphology of phase for new irregular bulky particles presence on the surface (Fig. 4(b,c)). This lead to increase in surface texture protuberance and coarseness, and thus increasing the surfaces area of the absorbents that facilitate the water diffusion into the absorbent. FE-SEM of adsorbent was taken before and after dye adsorption on (SA-g-(PAAC-co-VBS)/ZnO) surface.

The physical structure of zinc oxide clearly noticed as the ZnO nanoparticles were linked to the outer and inner surfaces and filled the cracks and holes in the sample of SA-g-(PAAC-co-VBS).

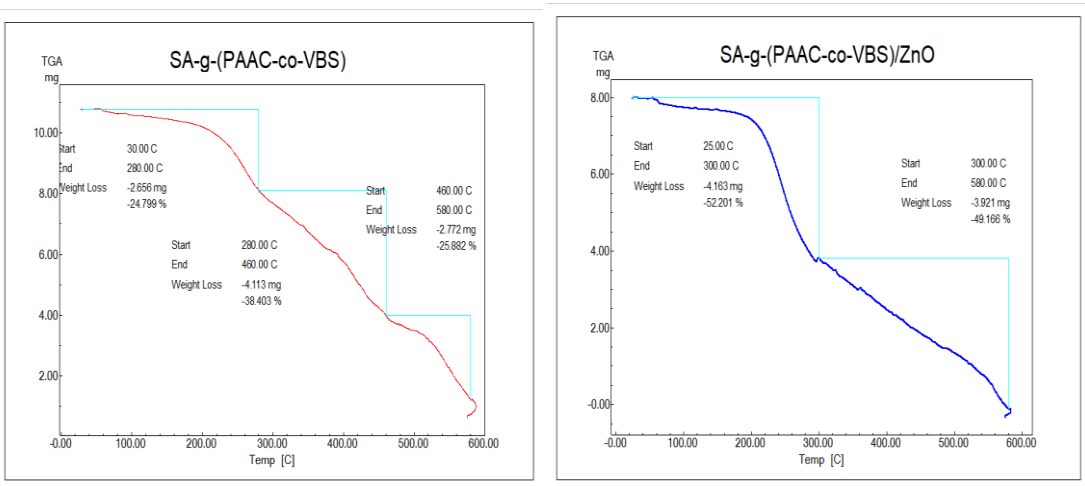

Fig. 3. TGA curve of the as-obtained like a) SA-g-(PAAC-co-VBS), b) SA-g-(PAAC-co-VBS)/ZnO NPs

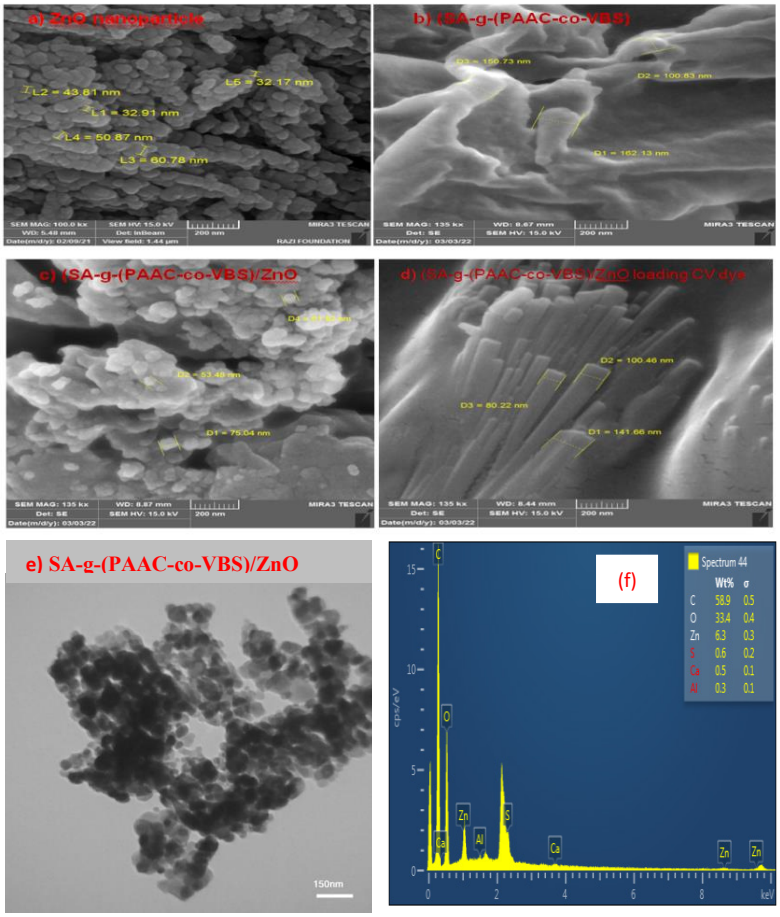

Fig. 4. FE-SEM images of (a) ZnO NPs, (b) SA-g-(PAAC-co-VBS), (c) SA-g-(PAAC-co-VBS)/ ZnONPs , (d) CV loaded SA-g-(PAAC-co-VBS)/ZnO NPs, (e) TEM images of SA-g-(PAAC-co-VBS) NPs and (f) EDS of SA-g-(PAAC-co-VBS) NPs.

Therefore, the spherical-like shape of ZnO NPs could be considered to enhance the uptake of CV dye because of the enhancement of the surface area of SA-g-(PAAC-co-VBS) [17]. In the morphology of SA-g-(PAAC-co-VBS)/ZnO, the internal pores can be seen which favors the intra-particle diffusion of CV as appears in fig. 4d. ZnO NPs provided well-developed pores with a uniform distribution that led to a porous structure and large surface area. The pores and surface of SA-g-(PAAC-co-VBS)/ZnO were entirely occupied by CV, and this confirms the successful adsorption process. Fig. 4e shows the TEM images of SA-g-(PAAC-co-VBS)/ZnO, where ZnO NPs observed embedded inside the SA-g-(PAAC-co-VBS). Also, the incorporation of ZnO NPs into SA-g-(PAAC-co-VBS) is confirmed by the presence of Zn and O peaks in the EDS of SA-g-(PAAC-co-VBS)/ZnO as shown in Fig.4f [32]. The synthesized nanocomposite contains C, O, Zn, S, Ca, and, Al elements, which confirms the presence of ZnO onto SA-g-(PAAC-co-VBS)/ZnO. The values of the highest and lowest elements that existed in the modified SA-g-(PAAC-co-VBS)/ZnO were 63.4 wt.% and 0.3 wt.%, respectively [33].

XRD analysis

The XRD spectra of ZnO NPs, SA-g-(PAAC-co-VBS)/ZnONPs, and SA-g-(PAAC-co-VBS) are shown in Fig. 5. The ZnO NPs crystalline peaks that appear at 32°, 34°, and 36° confirm the presence of ZnO NPs. The broadening in the peak is due to graft co-polymerization in the chains of poly acrylic acid onto SA [34]. The vanishing of crystalline peaks was observed after the addition of ZnO NPs to the hydrogel. The conversion from crystalline to amorphous phase may be due to the diffusion of

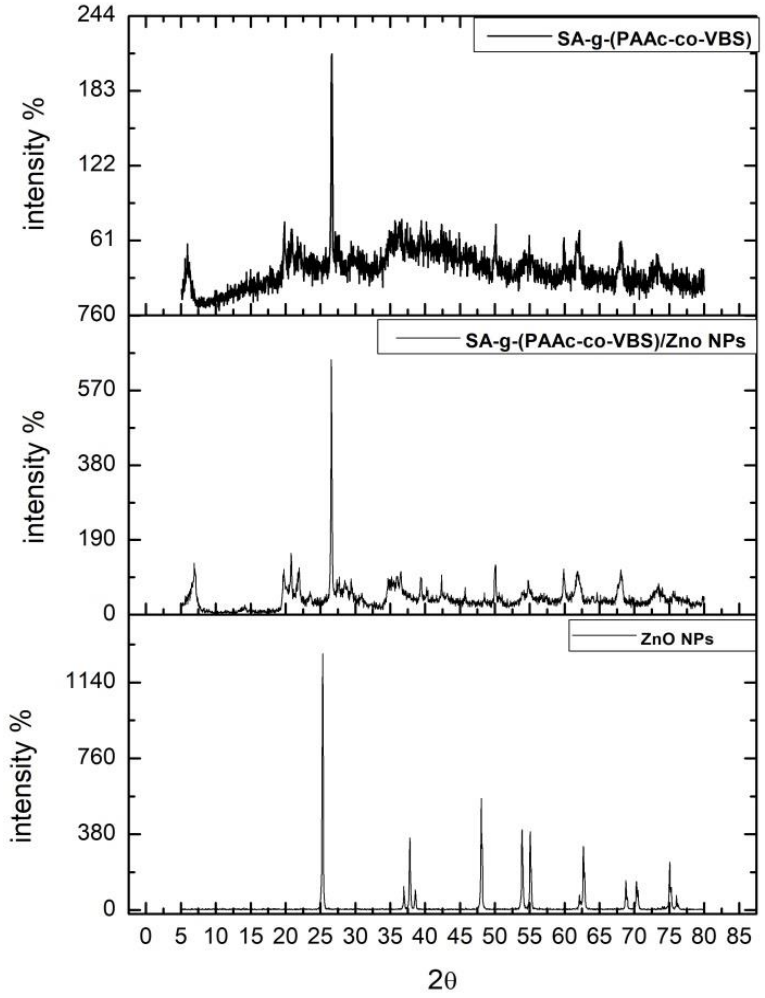

Fig. 5. X-ray diffraction patterns of (a) ZnO NPs, (b) SA-g-(PAAC-co-VBS)/ZnO NPs, and (c) SA-g-(PAAC-co-VBS).

ZnO NPs into the micro-pores and macro-pores of SA-g-(PAAC-co-VBS)/ZnONPs. The XRD patterns of SA-g-(PAAC-co-VBS)/ZnO NPs showed a very little peak observed in the case of ZnO which confirm the incorporation of ZnO NPs within the SA-g-(PAAC-co-VBS) matrix [35].

Adsorption process

Effect of contacting time

The contacting time is one of the significant parameters in the assessment of the practical application of the adsorption process. The experimental results of adsorption of chosen CV dye concentration 200 mg.L^{-1} on the adsorbent surfaces of the (SA-g-(PAAC-co-VBS)/ZnO) with contact time (Fig. 6) revealed that the adsorption increased quickly during the first 15 min, and then gradually till the equilibrium [36]. Also, the adsorption capacity increases with the increase of contacting time till reaches the equilibrium, which is come from the saturation of the active sites of absorbent surfaces. An acceptable efficiency was found at a contact time of two hours and a concentration of 200 mg.L-1, as the increase in time will have a slight effect on the removal rate due to the saturation of the active sites [37, 38].

Effect of the adsorbent dose

Investigation of the removal percentage E% of CV dye on the adsorbent dose of hydrogel was performed with unadjusted pH using several doses (0.01- 0.1 g) of SA-g-(PAAC-co-VBS)/ZnO at a

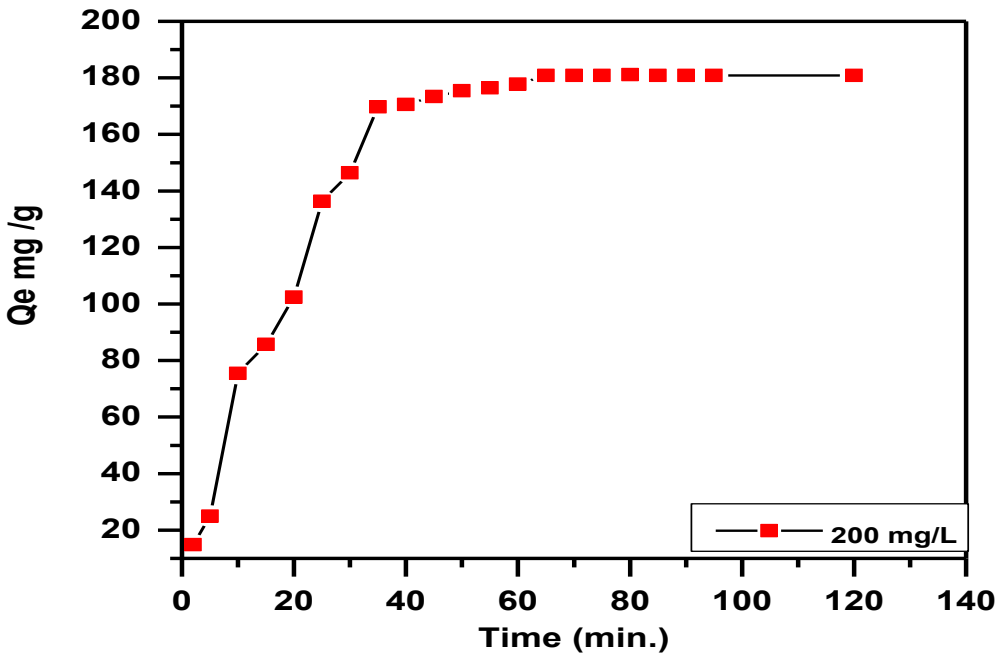

Fig. 6. Effect of contacting time on adsorption capacity for removal of CV dye by (SA-g-(PAAC-co-VBS)/ZnO) at pH = 6.6, Temp.= 30 °C, and mass adsorbent 0.04 g .

constant concentration of CV dye of 200 mg L^{-1}. The amount of adsorbed CV dye decreased from 200 to 159 mg/g, with increasing of adsorbents dosage from 0.01 to 0.1 g, and the removal efficiency E% of CV dye increased from 73.4 to 99.6% (Fig. 7). The incremental dye removal becomes constant of the adsorbent SA-g-(PAAC-co-VBS)/ZnO at amounts more than 0.04 g as the amount of dye in the solution diminished because of semi-stable removal, thus the chosen optimum dose of the adsorbents was 0.04 g. Increasing the adsorption percentage with increasing adsorbent dose can be attributed to the increased adsorbent surface area which leads to increasing of adsorption sites [21, 39, 40].

Effect of pH

Initial pH is an important factor in adsorption as it plays the main role in the protonation of functional groups, and in changing the surface charge of the adsorbent [17]. As shown in Fig 8, when the pH increases from 3 to 6.6, the adsorption capacity increases significantly, then followed by a slight decrease with the pH continuously increasing from 6.6 to 10. Complete removal of CV dye at the concentration of 200 mg.L^{-1} (100 mL) is achieved at pH= 6.6, and can reach the adsorption capacity of about 452.2 mg/g [41]. This is attributed to the de-protonation of functional groups in SA-g-(PAAC-co-VBS)/ZnO at this pH, which can simplify the electrostatic adsorption towards CV dye. It is worth to be mentioned that despite the adsorption behavior of CV has been weakened in the extremely acidic solution (pH= 3), the adsorption efficiency is still as high as 55.5 mg/g, which is better than the most common use adsorbents [40].

Kinetics model

The adsorption kinetics model is a very important factor to estimate the rate-controlling step and adsorption mechanism. Thus, the three utmost widely utilized adsorption kinetics the first model, the second model, and the Elkovich model are applied to further analyze the adsorption result. Their nonlinear equations calculate as follows [42]:

$$qt=qe[1-\exp(kf\,t)] \quad (3)$$

$$qt=\frac{K2qe2t}{1+K2qet} \quad (4)$$

$$qt=\frac{1}{\beta}1\beta\ln(\alpha\beta)+\frac{1}{\beta}\ln t \quad (5)$$

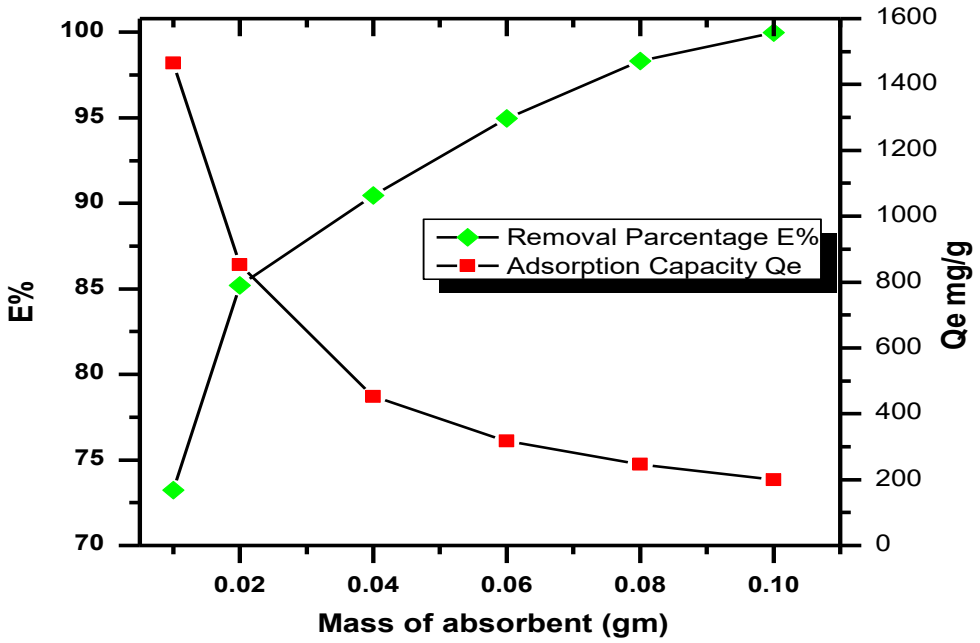

Fig. 7. Effect of the amount of adsorbent (SA-g-(PAAC-co-VBS)/ZnO) on the percent removal and amount of adsorbed CV dye, initial concentration = 200 mg.L^{-1}, Temp. = 30°C, contact time 2 h, and pH= 6.6.

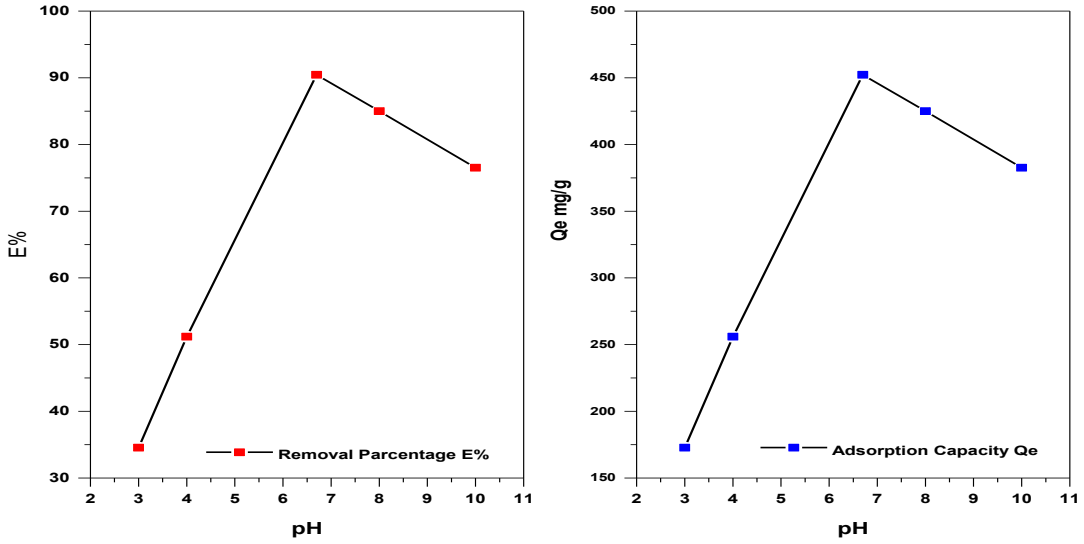

Fig. 8. Effect of pH on CV dye adsorption on (SA-g-(PAAC-co-VBS)/ZnO) (Exp. Condition: Temp.= 30°C, equilibrium time 1 h, and pH= 6.6).

where qt is the total amount of adsorbate that is adsorbed at time t (mg-1), qe is the equilibrium adsorption potential (mg. g^{-1}), kf is the rate constant of the first model (min^{-1}), and t is the contact time (min). k_2 is the second-order rate constant. The fitted parameters of the adsorption kinetics model of CV (200 mg/L) at 30 °C were calculated from the non-linear regressions of the integrated Eqs. (8-10)[43]. The study of the fitted curve of the kinetics model of dye is shown in Fig. 9 and Table 1.

The related factors and correlation coefficients

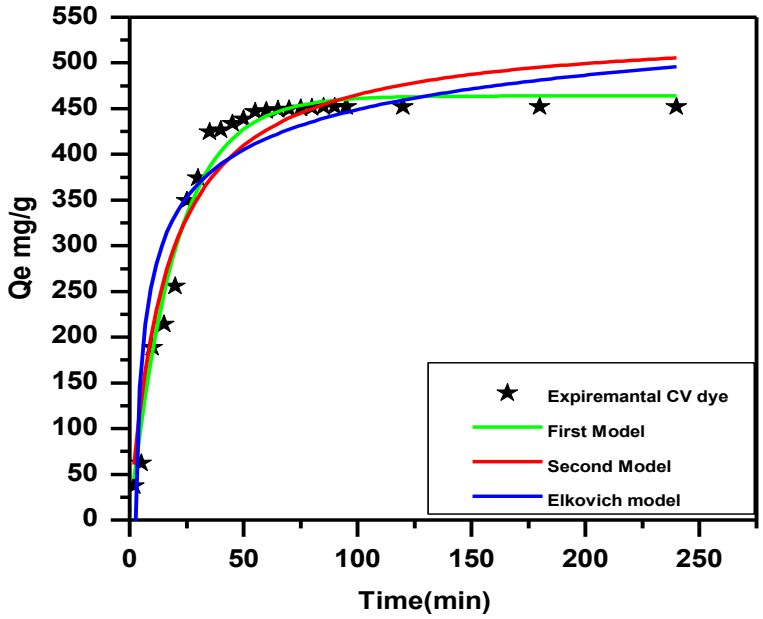

Fig. 9. The curve adsorption rate models fitted to experimental CV dye adsorption on the surface of (SA-g-(PAAC-co-VBS)/ZnO). a) kinetic first model ; b) kinetic second model ; and c) kinetic Elkovich model .

Table 1. Pseudo first-order, pseudo-second-order, and Elkovich including correlation coefficients for (CV dye) adsorption onto (SA-g-(PAAC-co-VBS)/ZnO).

Type	Parameters	Value	Stand. Error	*R*2
Pseudo-First-order	qe (mg g^{-1})	463.86	6.659	0.9774
	k*f* (min^{-1})	0.0508	0.003	
pseudo-second-order	qe (mg g^{-1})	538.69	19.83	0.9311
	ks (gmg^{-1} min^{-1})	0.063	0.0089	
Elkovich	α (mg g^{-1} min^{-1})	268.60	24.042	0.8491
	β (g min^{-1})	1.155	0.151	

(R_2=0.9977), (R_2=0.9315), and (R_2=0.843) can be obtained via the regression of the experimental results. The values of q_e are pretty close to q_{exp} of the first model, comparative to the sound and Elkovich model indicating that the adsorption process of CV dye onto the adsorbents fitted the first model. Also, the correlation coefficient obtained from the equation First model was equal to 0.9977, which further proposed that the total adsorption process of the SA-g-(PAAC-co-VBS)/ ZnO obeyed the kinetic First model [44, 45].

Adsorption Isotherm

Adsorption results are utmost often represented by the value of the equilibrium isotherm, in which the adsorption capacity (q_e mg/g) is the concentration of the sorbent (the solid-phase) versus the concentration of the sorbate in the liquid phase (Ce mg/L). At the point of dynamic isotherm of the adsorption method, there is a requirement to determine the adsorbate spreading amidst the solid phase and liquid phase; this information can be gutted through adsorption equilibrium studies. In this study, two of the utmost generally utilized isotherms, namely the isotherm Langmuir and isotherm Freundlich were utilized to describe the adsorption isotherm. The non-linear forms of the Langmuir and Freundlich

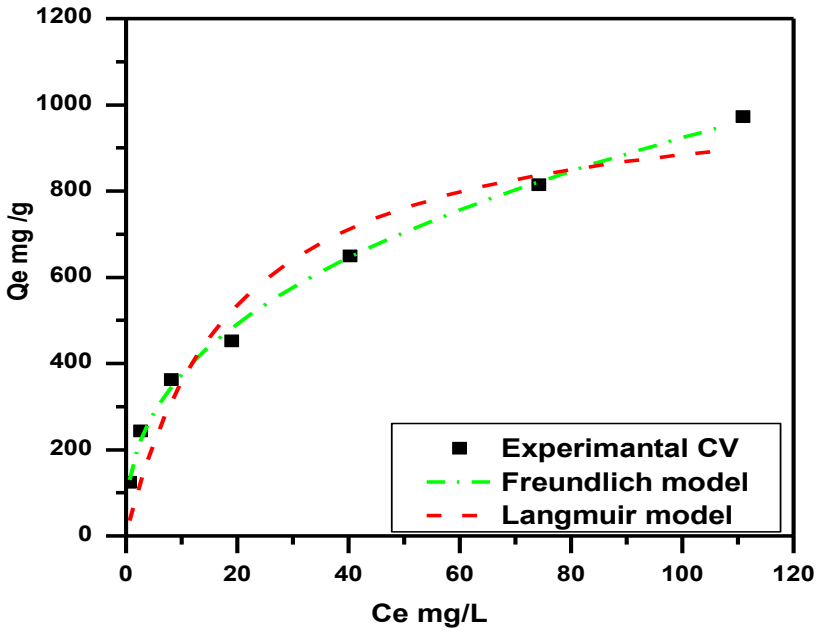

Fig. 10. Several adsorptions models nonlinear fit of adsorption CV onto (SA-g-(PAAC-co-VBS)/ ZnO) at temperatures 30 °C , conc. = 200 mg. L^{-1}, pH of solution 6.6 and weight of surface 0.04 g/100ml).

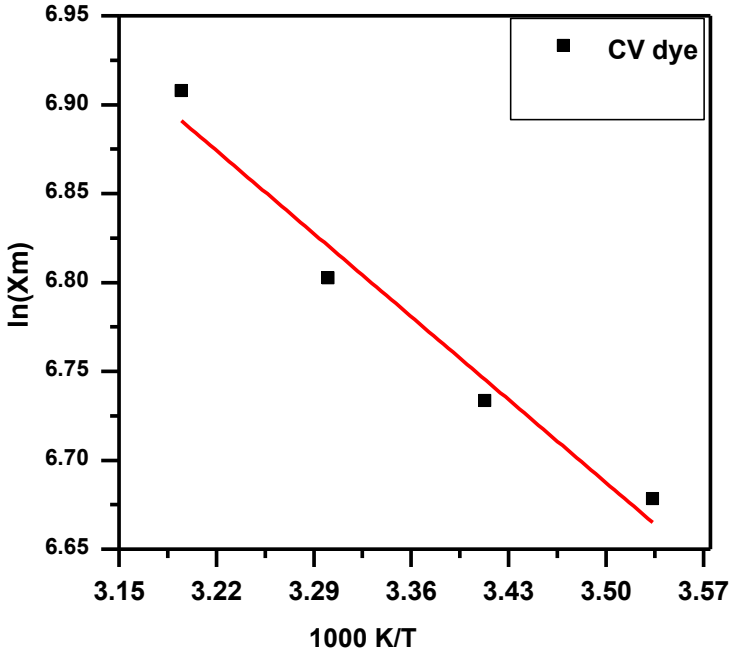

Figure 11. Van't Hoff plot used to determine thermodynamic parameters.

models [46, 47] are given as:

$$q_e = \frac{q_m K_L C_e}{1+K_L C_e} \quad (6)$$

$$q_e = K_f C_e^{1/n} \quad (7)$$

qe: The amount of adsorbed per unit weight

Table 2. Thermodynamic Parameter ΔG, ΔS and, ΔH of CV dye adsorbed on the (SA-g-(PAAC-co-VBS)/ZnO).

T/K	K_{eq}	-ΔG°/kJ.mol^{-1}	ΔH°/kJ.mol^{-1}	ΔS°/J.K^{-1}.mol^{-1}
283.15	8457.447	21.2765	5.548	75.012
293.15	8936.17	22.1624		
303.15	9574.468	23.0926		
313.15	10638.3	24.1289		

(mg/g) of adsorbent at equilibrium. Ce: Concentration of adsorbate in solution after adsorption at equilibrium (mg.L-1), (mol/L). qm is the empirical Langmuir constant that represents the maximum adsorption capacity (mg/g) of the total number of surface sites per mass of adsorbent. It may vary in different compounds because of differences in adsorbate sizes. KL: Empirical Langmuir constant (L/mg) or the equilibrium constant of the adsorption reaction. Kf: Empirical Freundlich constant or capacity factor (L/mg) or the dye quantity adsorbed for unit equilibrium concentration. 1/n: Freundlich exponent, if n=1, the adsorption is linear; if n<1, then the adsorption is chemical, and if the value is more than 1, then the adsorption will be physical [48-50].

A plot of qe vs Ce (Fig. 10), where the values of KF and 1/n are obtained from the intercept and slope in the same order. The correlation coefficient (R_2) value for the Freundlich model at 30 °C is R_2= 0.9969 of CV onto (SA-g-(PAAC-co-VBS)/ZnO) [51, 52].

Thermodynamic Study

The results obtained from the study of temperature were utilized for the thermodynamic parameters. Gibbs free energy (ΔG^o) is presented in Eq. 5, which can be well expressed by means of ΔH and ΔS, at a constant temperature (Eq. 6). The linearized form of equations 5 and 6 results in Eq. 7, which is the van't Hoff equation:

$$\Delta G = -RT \ln Ke \quad (8)$$

$$\Delta G = \Delta H - T\Delta S \quad (9)$$

$$\ln X_m = -\frac{\Delta H^\circ}{RT} + \frac{\Delta S^\circ}{R} \quad (10)$$

where ΔG° (kJ/mol) changes in Gibbs free Energy, ΔH° (kJ/mol) changes in enthalpy, ΔS° (J/mol. K) changes in the entropy of CV dye adsorption, R gas constant (8.314J/mol K), T absolute temperature (K).

The data reveals that the equilibrium adsorption efficiency of CV dye was increased with the increasing temperature of the solution for all initial concentrations [53]. The values of ΔH and ΔS respectively can be calculated from the slope and intercept of vant Hoff equation by plotting of ln Xm vs 1000 K/T (Fig. 11). The thermo-dynamic parameters are given in Table 2.

As shown in the table, the ΔG ^{o} values are negative for SA-g-(PAAC-co-VBS)/ZnO, which indicates the spontaneous nature of the sorption method. For all the sorbents, the positive value of ΔH suggests the endothermic nature of the adsorption method. Moreover, the positive values of ΔS indicate the increase in randomness at the interface of solid/liquid during the sorption of CV onto SA-g-(PAAC-co-VBS)/ZnO [54].

Regeneration of (SA-g-(PAAC-co-VBS)/ZnO).

The regeneration of hydrogels after sorption is one of the economically significant parameters. It aids in predicting the mechanism of CV dye removal from dye-loaded adsorbents, and recycling of used adsorbents, which in turn may reduce the costs and protect the environment from secondary pollution. For the desorption studies of CV, different agents were used at 0.01 N such as H_2SO_4, NaOH, H_3PO_4, HCl, HNO_3, and water [55-58]. The synthesized adsorbent (SA-g-(PAAC-co-VBS)/ZnO) was regenerated with 100% in a diluted HCl solution. This is because of the conversion of –COO− to –COOH in acidic solutions which leads to the weakening of the electrostatic interactions between (SA-g-(PAAC-co-VBS)/ZnO) and CV.

The reusability and performance of (SA-g-(PAAC-co-VBS)/ZnO) after adsorption of CV dye were investigated using HCl solution for up to 3 steps under optimum conditions. After the 3 cycles of using the adsorbent SA-g-(PAAC-co-VBS)/ZnO,

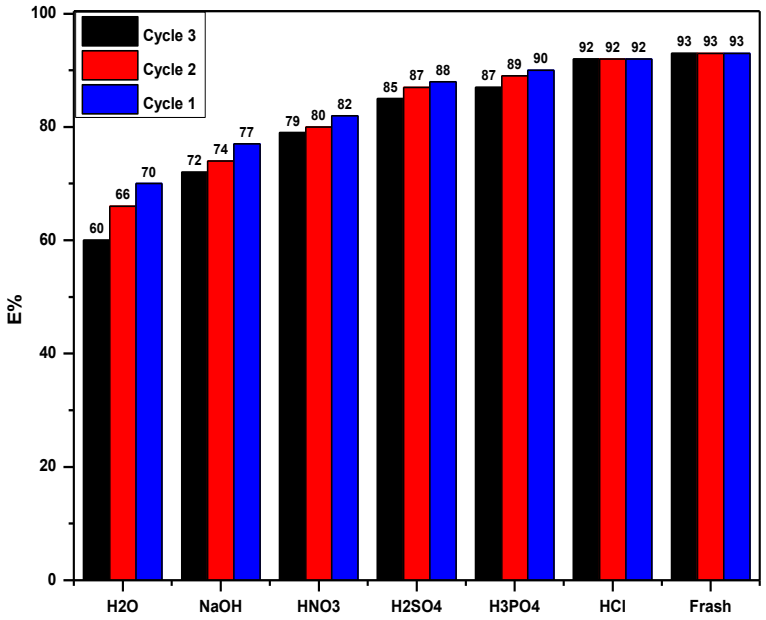

Fig. 12: Comparison of CV dye removal efficiency (%) using fresh and three cycles regenerated (SA-g-(PAAC-co-VBS)/ZnO).

the efficiency is still significant (>80%) and this reveals that SA-g-(PAAC-co-VBS)/ZnO is a probable renewable adsorber [32, 59] as shown in Fig. 12.

CONCLUSION

In the current research, we report the synthesis of the new superabsorbent (SA-g-(PAAC-co-VBS)/ZnO) using the free radical graft copolymerization method. Characterization techniques revealed the presence of ZnO in the hydrogel matrix which was confirmed via FT-IR and XRD. Introducing ZnO NPs into the hydrogel matrix of SA and AAC grafted onto VBS resulted in a unique structure, high pore volume, and high surface area which led to a high adsorption efficiency of superabsorbent. The superabsorbent exhibited good capacities for CV removal from an aqueous solution, as it successfully removed about 98.9%. The kinetics model result fits well with the model First-order, and the adsorption mechanism was controlled by intraparticle diffusion as well as boundary layer diffusion. The isotherm model which followed by the adsorption process in this work is Freundlich one with a maximum adsorption efficiency about of 1150 mg/g. The adsorption method was found to be spontaneous and endothermic physical adsorption. Hence, the synthesized adsorbents can be used effectively in the water treatment for removal of selective cationic dyes. Furthermore, desorption studies predicted that the superabsorbent can be utilized repeatedly for the regeneration of CV dye. In summary, the superabsorbent has the potential to be utilized as an environmentally friendly and efficient adsorbent for the removal of CV from an aqueous solution.

CONFLICT OF INTEREST

The authors declare that there is no conflict of interests regarding the publication of this manuscript.

REFERENCE

1. Inyinbor AA, Adekola FA, Olatunji GA. Adsorption of Rhodamine B dye from aqueous solution on Irvingia gabonensis biomass: Kinetics and thermodynamics studies. South African Journal of Chemistry. 2015;68.
2. Li S, Tang Y, Zhang J, Hao W, Chen W, Gu F, et al. Advanced and green ozonation process for removal of clofibric acid in water system: Preparation and mechanism analysis of efficient copper-substituted MCM-48. Separation and Purification Technology. 2019;211:684-696.
3. Nariyan E, Aghababaei A, Sillanpää M. Removal of pharmaceutical from water with an electrocoagulation process; effect of various parameters and studies of isotherm and kinetic. Separation and Purification Technology. 2017;188:266-281.
4. Heo J, Kim H, Her N, Lee S, Park Y-G, Yoon Y. Natural organic matter removal in single-walled carbon nanotubes–ultrafiltration membrane systems. Desalination. 2012;298:75-84.

5. Pérez-Armada L, Rivas S, González B, Moure A. Extraction of phenolic compounds from hazelnut shells by green processes. Journal of Food Engineering. 2019;255:1-8.
6. Alkaim AF, Abdulrazzak FH, Essa SM, Altimari US, Ramadan MF, Aljeboree AM. Methacrylic Acid-Acrylamide based ZnO Hydrogel Nanocomposite Assisted Photocatalytic Decolorization of Methylene Blue Dye. INTERNATIONAL JOURNAL OF PHARMACEUTICAL QUALITY ASSURANCE. 2023;14(02):279-282.
7. Removal of Pharmaceutical Amoxicillin drug by using (CNT) decorated Clay/ Fe_2O_3 Micro/Nanocomposite as effective adsorbent: Process optimization for ultrasound-assisted adsorption. International Journal of Pharmaceutical Research. 2019;11(4).
8. Roy D, Cambre JN, Sumerlin BS. Future perspectives and recent advances in stimuli-responsive materials. Progress in Polymer Science. 2010;35(1-2):278-301.
9. Ahmed EM, Aggor FS, Awad AM, El-Aref AT. An innovative method for preparation of nanometal hydroxide superabsorbent hydrogel. Carbohydrate Polymers. 2013;91(2):693-698.
10. Singh RK, Sharma HO, Garg SK. Interpretive structural modelling for selection of best supply chain practices. International Journal of Business Performance and Supply Chain Modelling. 2010;2(3/4):237.
11. Sikareepaisan P, Ruktanonchai U, Supaphol P. Preparation and characterization of asiaticoside-loaded alginate films and their potential for use as effectual wound dressings. Carbohydrate Polymers. 2011;83(4):1457-1469.
12. Roufegari-Nejhad E, Sirousazar M, Abbasi-Chiyaneh V, Kheiri F. Removal of Methylene Blue from Aqueous Solutions Using Poly(vinyl alcohol)/Montmorillonite Nanocomposite Hydrogels: Taguchi Optimization. Journal of Polymers and the Environment. 2019;27(10):2239-2249.
13. Jawad AH, Mubarak NSA, Abdulhameed AS. Hybrid Crosslinked Chitosan-Epichlorohydrin/TiO_2 Nanocomposite for Reactive Red 120 Dye Adsorption: Kinetic, Isotherm, Thermodynamic, and Mechanism Study. Journal of Polymers and the Environment. 2019;28(2):624-637.
14. Jawad AH, Abdulhameed AS, Kashi E, Yaseen ZM, Alothman ZA, Khan MR. Cross-linked chitosan-glyoxal/kaolin clay composite: Parametric optimization for color removal and COD reduction of remazol brilliant blue R dye. Research Square Platform LLC; 2021.
15. Aljeboree AM, Radia ND, Jasim LS, Alwarthan AA, Khadhim MM, Washeel Salman A, et al. Synthesis of a new nanocomposite with the core TiO2/hydrogel: Brilliant green dye adsorption, isotherms, kinetics, and DFT studies. Journal of Industrial and Engineering Chemistry. 2022;109:475-485.
16. Malik AQ, Mir TuG, Amin O, Sathish M, Kumar D. Synthesis, characterization, photocatalytic effect of CuS-ZnO nanocomposite on photodegradation of Congo red and phenol pollutant. Inorganic Chemistry Communications. 2022;143:109797.
17. Thakur S, Arotiba O. Synthesis, characterization and adsorption studies of an acrylic acid-grafted sodium alginate-based TiO_2 hydrogel nanocomposite. Adsorption Science & Technology. 2017;36(1-2):458-477.
18. Al-Musawi TJ, Mengelizadeh N, Taghavi M, Mohebi S, Balarak D. Activated carbon derived from Azolla filiculoides fern: a high-adsorption-capacity adsorbent for residual ampicillin in pharmaceutical wastewater. Biomass Conversion and Biorefinery. 2021.
19. Zhao Y, Chen Y, Zhao J, Tong Z, Jin S. Preparation of SA-g-(PAA-co-PDMC) polyampholytic superabsorbent polymer and its application to the anionic dye adsorption removal from effluents. Separation and Purification Technology. 2017;188:329-340.
20. Mohammad N, Atassi Y, Tally M. Synthesis and swelling behavior of metal-chelating superabsorbent hydrogels based on sodium alginate-g-poly(AMPS-co-AA-co-AM) obtained under microwave irradiation. Polymer Bulletin. 2017;74(11):4453-4481.
21. Oladipo AA, Gazi M. Enhanced removal of crystal violet by low cost alginate/acid activated bentonite composite beads: Optimization and modelling using non-linear regression technique. Journal of Water Process Engineering. 2014;2:43-52.
22. Cass P, Knower W, Pereeia E, Holmes NP, Hughes T. Preparation of hydrogels via ultrasonic polymerization. Ultrasonics Sonochemistry. 2010;17(2):326-332.
23. Gharehbakhsh H, Panahi HA, Toosi MR, Hassani AH, Moniri E. Application of polyamide thin-film composite layered on polysulfone-GO/TiO_2 mixed matrix membranes for removal of nitrotoluene derivatives from petrochemical wastewaters. Environmental Science and Pollution Research. 2020;27(34):42481-42494.
24. Luo S, Liu C, Zhou S, Li W, Ma C, Liu S, et al. ZnO nanorod arrays assembled on activated carbon fibers for photocatalytic degradation: Characteristics and synergistic effects. Chemosphere. 2020;261:127731.
25. Yasin AS, Kim Dh, Lee K. One-pot synthesis of activated carbon decorated with ZnO nanoparticles for capacitive deionization application. Journal of Alloys and Compounds. 2021;870:159422.
26. De Luca P, B. Nagy J. Treatment of Water Contaminated with Reactive Black-5 Dye by Carbon Nanotubes. Materials. 2020;13(23):5508.
27. Guo Y, Wang H, He C, Qiu L, Cao X. Uniform Carbon-Coated ZnO Nanorods: Microwave-Assisted Preparation, Cytotoxicity, and Photocatalytic Activity. Langmuir. 2009;25(8):4678-4684.
28. Xiong H-M, Xu Y, Ren Q-G, Xia Y-Y. Stable Aqueous ZnO@Polymer Core–Shell Nanoparticles with Tunable Photoluminescence and Their Application in Cell Imaging. Journal of the American Chemical Society. 2008;130(24):7522-7523.
29. Zhou X, Li Y, Peng T, Xie W, Zhao X. Synthesis, characterization and its visible-light-induced photocatalytic property of carbon doped ZnO. Materials Letters. 2009;63(20):1747-1749.
30. Zhou M, Gao X, Hu Y, Chen J, Hu X. Uniform hamburger-like mesoporous carbon-incorporated ZnO nanoarchitectures: One-pot solvothermal synthesis, high adsorption and visible-light photocatalytic decolorization of dyes. Applied Catalysis B: Environmental. 2013;138-139:1-8.
31. Banerjee S, Chattopadhyaya MC. Adsorption characteristics for the removal of a toxic dye, tartrazine from aqueous solutions by a low cost agricultural by-product. Arabian Journal of Chemistry. 2017;10:S1629-S1638.
32. Mittal H, Al Alili A, Morajkar PP, Alhassan SM. Graphene oxide crosslinked hydrogel nanocomposites of xanthan gum for the adsorption of crystal violet dye. Journal of Molecular Liquids. 2021;323:115034.
33. El Shafey AM, Abdel-Latif MK, Abd El-Salam HM. The facile synthesis of poly(acrylate/acrylamide) titanium dioxide

nanocomposite for groundwater ammonia removal. DESALINATION AND WATER TREATMENT. 2021;212:61-70.
34. Ahmed IA, Seliem MK, Lima EC, Badawi M, Li Z, Bonilla-Petriciolet A, et al. Outstanding Performance of a New Exfoliated Clay Impregnated with Rutile TiO_2 Nanoparticles Composite for Dyes Adsorption: Experimental and Theoretical Studies. Coatings. 2021;12(1):22.
35. Gharehbakhsh H, Ahmad Panahi H, Toosi MR, Hassani AH, Moniri E. Adsorptive removal of toluenediamine from aqueous solution by polysulfone/graphene oxide/TiO_2 membrane functionalized by allylamine. Chemical Data Collections. 2022;37:100800.
36. Shahul Hameed K, Muthirulan P, Meenakshi Sundaram M. Adsorption of chromotrope dye onto activated carbons obtained from the seeds of various plants: Equilibrium and kinetics studies. Arabian Journal of Chemistry. 2017;10:S2225-S2233.
37. Yazidi A, Atrous M, Edi Soetaredjo F, Sellaoui L, Ismadji S, Erto A, et al. Adsorption of amoxicillin and tetracycline on activated carbon prepared from durian shell in single and binary systems: Experimental study and modeling analysis. Chemical Engineering Journal. 2020;379:122320.
38. Chkirida S, Zari N, Achour R, Hassoune H, Lachehab A, Qaiss Aek, et al. Highly synergic adsorption/photocatalytic efficiency of Alginate/Bentonite impregnated TiO_2 beads for wastewater treatment. Journal of Photochemistry and Photobiology A: Chemistry. 2021;412:113215.
39. Aljeboree AM, Alkaim AF. Removal of Antibiotic Tetracycline (TCs) from aqueous solutions by using Titanium dioxide (TiO_2) nanoparticles as an alternative material. Journal of Physics: Conference Series. 2019;1294(5):052059.
40. Gao B, Yu H, Wen J, Zeng H, Liang T, Zuo F, et al. Super-adsorbent poly(acrylic acid)/laponite hydrogel with ultrahigh mechanical property for adsorption of methylene blue. Journal of Environmental Chemical Engineering. 2021;9(6):106346.
41. Bonetto LR, Ferrarini F, de Marco C, Crespo JS, Guégan R, Giovanela M. Removal of methyl violet 2B dye from aqueous solution using a magnetic composite as an adsorbent. Journal of Water Process Engineering. 2015;6:11-20.
42. Aljeboree AM, Mohammed RA, Mahdi MA, Jasim LS, Alkaim AF. Synthesis, Characterization of P(CH/AA-co-AM) and Adsorptive Removal of Pb (II) ions from Aqueous Solution: Thermodynamic Study. NeuroQuantology. 2021;19(7):137-143.
43. Al-Lami HS, Abdulwahid AA, Mizhir AA. Adsorption process for removing hazardous Congo red dye from aqueous solutions: isotherm, kinetic, and thermodynamic studies. DESALINATION AND WATER TREATMENT. 2022;280:177-187.
44. Zaheer Z, Al-Asfar A, Aazam ES. Adsorption of methyl red on biogenic Ag@Fe nanocomposite adsorbent: Isotherms, kinetics and mechanisms. Journal of Molecular Liquids. 2019;283:287-298.
45. Liu Y, Chen Y, Shi Y, Wan D, Chen J, Xiao S. Adsorption of toxic dye Eosin Y from aqueous solution by clay/carbon composite derived from spent bleaching earth. Water Environment Research. 2020;93(1):159-169.
46. Kim Y-S, Kim J-H. Isotherm, kinetic and thermodynamic studies on the adsorption of paclitaxel onto Sylopute. The Journal of Chemical Thermodynamics. 2019;130:104-113.
47. Siva K, Asif, Poulose, Suguna, Al H. Equilibrium and Kinetic Studies of Biosorptive Removal of 2,4,6-Trichlorophenol from Aqueous Solutions Using Untreated Agro-Waste Pine Cone Biomass. Processes. 2019;7(10):757.
48. Dil EA, Ghaedi M, Ghaedi AM, Asfaram A, Goudarzi A, Hajati S, et al. Modeling of quaternary dyes adsorption onto ZnO–NR–AC artificial neural network: Analysis by derivative spectrophotometry. Journal of Industrial and Engineering Chemistry. 2016;34:186-197.
49. Gouamid M, Ouahrani MR, Bensaci MB. Adsorption Equilibrium, Kinetics and Thermodynamics of Methylene Blue from Aqueous Solutions using Date Palm Leaves. Energy Procedia. 2013;36:898-907.
50. Kayranli B. Adsorption of textile dyes onto iron based waterworks sludge from aqueous solution; isotherm, kinetic and thermodynamic study. Chemical Engineering Journal. 2011;173(3):782-791.
51. Aljeboree AM, Alshirifi AN, Alkaim AF. Kinetics and equilibrium study for the adsorption of textile dyes on coconut shell activated carbon. Arabian Journal of Chemistry. 2017;10:S3381-S3393.
52. Aljeboree AM, Alkaim AF, Al-Dujaili AH. Adsorption isotherm, kinetic modeling and thermodynamics of crystal violet dye on coconut husk-based activated carbon. Desalination and Water Treatment. 2014;53(13):3656-3667.
53. Yao Y, Bing H, Feifei X, Xiaofeng C. Equilibrium and kinetic studies of methyl orange adsorption on multiwalled carbon nanotubes. Chemical Engineering Journal. 2011;170(1):82-89.
54. Wang Y, Wang W, Wang A. Efficient adsorption of methylene blue on an alginate-based nanocomposite hydrogel enhanced by organo-illite/smectite clay. Chemical Engineering Journal. 2013;228:132-139.
55. Zhang G, Feizbakhshan M, Zheng S, Hashisho Z, Sun Z, Liu Y. Effects of properties of minerals adsorbents for the adsorption and desorption of volatile organic compounds (VOC). Applied Clay Science. 2019;173:88-96.
56. Hoppen MI, Carvalho KQ, Ferreira RC, Passig FH, Pereira IC, Rizzo-Domingues RCP, et al. Adsorption and desorption of acetylsalicylic acid onto activated carbon of babassu coconut mesocarp. Journal of Environmental Chemical Engineering. 2019;7(1):102862.
57. Al-Bayati RA, Ahmed AS. Adsorption – Desorption of Trimethoprim Antibiotic Drug from Aqueous Solution by Two Different Natural Occurring Adsorbents. International Journal of Chemistry. 2011;3(3).
58. Pashaei-Fakhri S, Peighambardoust SJ, Foroutan R, Arsalani N, Ramavandi B. Crystal violet dye sorption over acrylamide/graphene oxide bonded sodium alginate nanocomposite hydrogel. Chemosphere. 2021;270:129419.
59. Sukul P, Lamshöft M, Zühlke S, Spiteller M. Sorption and desorption of sulfadiazine in soil and soil-manure systems. Chemosphere. 2008;73(8):1344-1350.